Document ID: EDF-5741
Revision ID: 1
Effective Date: 04/25/2007

Engineering Design File

Advanced Gas Reactor-1 Pre-Test Prediction Analyses using the PARFUME Code

The INL is a U.S. Department of Energy National Laboratory
operated by Battelle Energy Alliance.

Idaho National Laboratory

ADVANCED GAS REACTOR-1 PRE-TEST PREDICTION ANALYSES USING THE PARFUME CODE	Identifier: EDF-5741 Revision: 1 Effective Date: 04/25/2007	Page: 1 of **29**

AGR-1	Technical Evaluation Study or Engineering Design File	**USE TYPE**	DAR Number: 550709

REVISION LOG

Rev.	Date	Affected Pages	Revision Description
1	04/25/2007	all	To incorporate updates to fuel specifications, nuclear physics, and thermal analyses.

1. INTRODUCTION

This engineering design file (EDF) documents analyses that were performed to predict fuel particle behavior and the probability of fuel particle failure during the first planned irradiation test of the Advanced Gas Reactor program (otherwise referred to as the AGR-1 test). These analyses were completed using the particle fuel model computer code known as PARFUME. It should be noted that this EDF represents a revision of the original work[1] based on updates to fuel specifications,[2] nuclear physics,[3] and thermal analyses.[4,5]

PARFUME, which is under development at the Idaho National Laboratory (INL), is an integrated mechanistic code that evaluates the thermal, mechanical, and physico-chemical behavior of fuel particles during irradiation and the probability for fuel failure given the particle-to-particle statistical variations in physical dimensions and material properties that arise from the fuel fabrication process. A more detailed description of the code is available in References 6 and 7. All calculations were performed on a Sun x86_64 workstation running SUSE LINUX using PARFUME Version 2.13[8] as configured in a Revision Control System (RCS).[9]

Although PARFUME results have been compared with hand calculations and with results from codes that have been subjected to formal verification and validation (V&V) programs, the V&V of PARFUME is not considered complete. This situation is unavoidable given that the code is still in the development stage. This is mentioned only as an indication of the current code status and should not be interpreted to mean that PARFUME results are unreliable or unusable. Comparisons against independent results have already instilled a level of confidence in the code.[10] In addition, PARFUME itself contains four independent failure probability solution schemes: one based on Monte Carlo techniques and three based on (full-loop, 3-loop, and 2-loop) integration algorithms. Results are routinely generated using all schemes and then compared as further evidence of code validity.

Details associated with completion of these analyses is provided in the remainder of this document. Specifically, a discussion of the PARFUME modeling is outlined in Section 2, results are described in Section 3, conclusions derived through the analyses are given in Section 4, and references are listed in Section 5.

2. MODELING

The large East “B” position in the Advanced Test Reactor (ATR) is the location for the AGR-1 test. The test includes a total of six capsules arranged vertically. A radial cross section through a single capsule inside the “B” position is shown in Figure 1. As indicated, each capsule contains three fuel stacks. Each fuel stack consists of a vertical arrangement of four fuel compacts. Consequently, a total of 12 fuel compacts are contained in each capsule (three stacks per capsule with four compacts per stack).

The capsule arrangement inside the “B” position is illustrated in the axial cross section provided in Figure 2. Only two of the three fuel stacks in each capsule are shown (the third fuel stack in each capsule is hidden behind the two stacks that are shown). Note that the horizontal division of each fuel compact is an aspect of modeling only and should not be interpreted to represent a physical segmentation of the compacts.

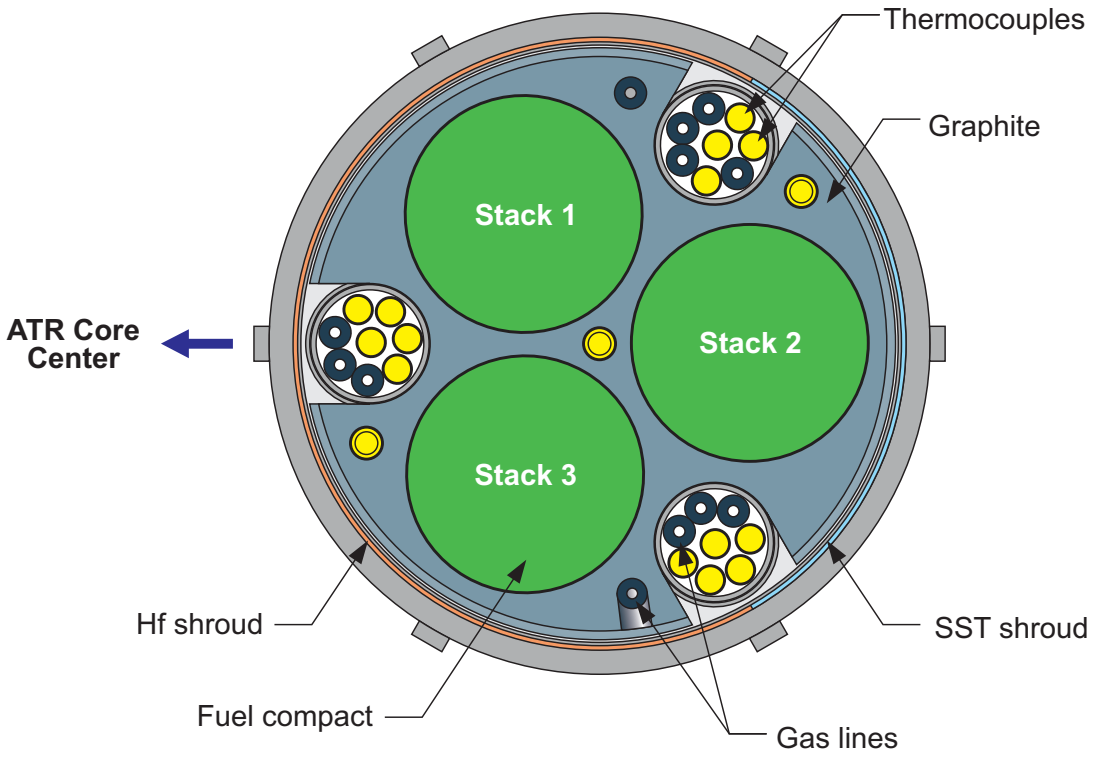

Figure 1. Radial cross section of a capsule in the AGR-1 test showing 3 vertical fuel stacks (not to scale).

Based on current specifications,[2] the fuel compacts are right circular cylinders measuring ~12.4 mm in diameter and ~25.1 mm tall. Each compact contains ~4000 fuel particles uniformly disbursed in a carbon-based substrate. Each particle has a nominal diameter of ~800 μm and contains a kernel consisting of UCO fuel. The kernel is coated with a porous buffer layer to accommodate fission product accumulation, a SiC layer to retain the fission products, and inner and outer pyrocarbon layers to protect the SiC as depicted in Figure 3. Capsule irradiation in ATR has been tentatively set at ~720 effective full power days (EFPD). Key aspects of the PARFUME modeling of these AGR-1 conditions are described below.

2.1. Boundary/Initial Conditions

PARFUME is designed to evaluate fuel performance based on user inputs for neutron fluence and burnup with a corresponding set of thermal conditions. Results from neutronics analyses and/or measured values are possible sources for fluence and burnup inputs. In this EDF, capsule-specific fluence and burnup results from neutronics analyses performed as part of the AGR-1 design effort were used as shown in Figures 4 and 5, respectively.[3]

PARFUME has considerable flexibility relative to the application of thermal conditions affecting fuel particles. A user may define thermal conditions for the outer surfaces of fuel bearing materials (i.e., the outer surface of a pebble in the case of a pebble bed reactor or the coolant channel surface of a unit cell containing fuel compacts in the case of a prismatic reactor) or the user may define fuel bearing material temperatures directly. Options for the outer surfaces of fuel bearing materials include defining either a

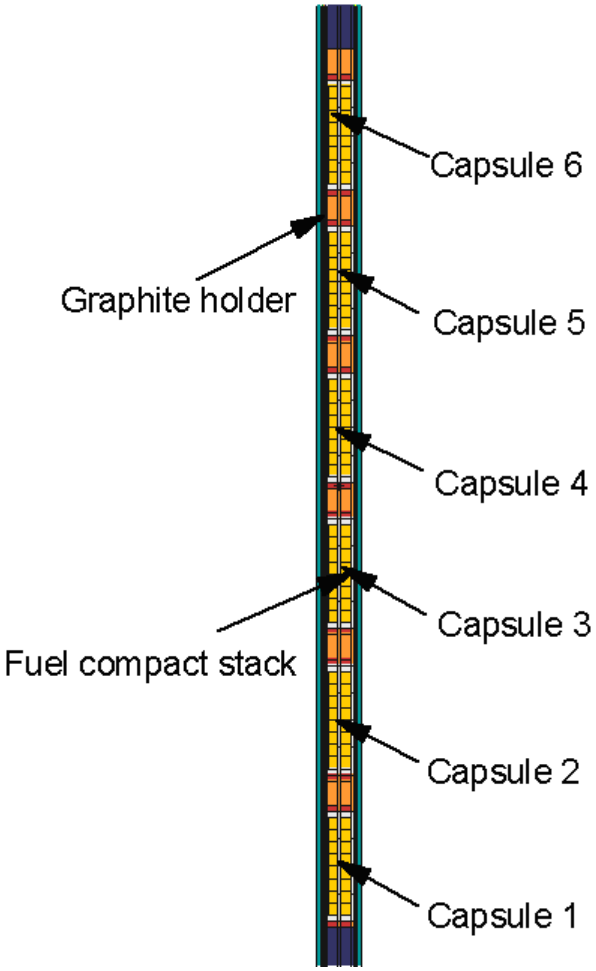

Figure 2. Axial cross section of the AGR-1 test showing two of the three vertical fuel stacks with each compact divided into halves for modeling purposes (not to scale).

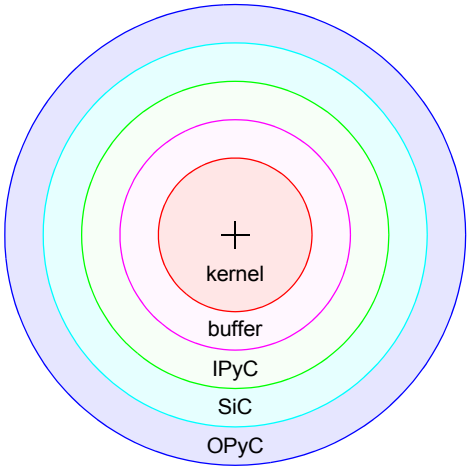

Figure 3. Cross section through a coated fuel particle (not to scale).

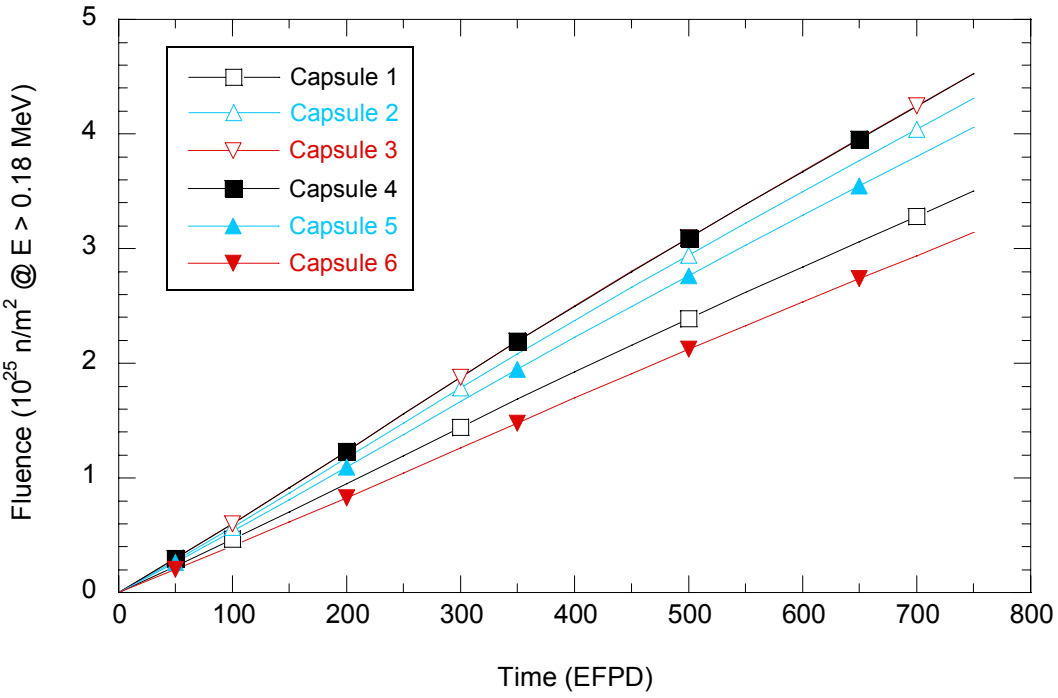

Figure 4. Fluence as a function of time from AGR-1 neutronics analyses.[3]

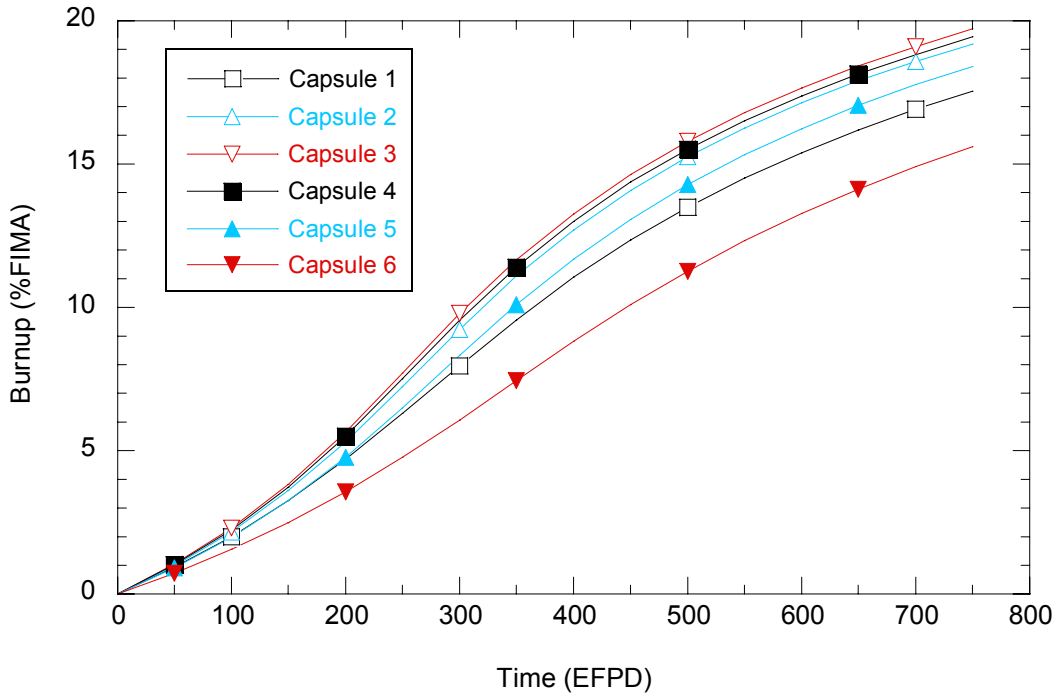

Figure 5. Burnup as a function of time from AGR-1 neutronics analyses.[3]

time-dependent set of temperatures or a time-dependent set of heat transfer coefficients with a corresponding time-dependent set of sink temperatures. Fuel bearing material temperatures can be defined directly as time-dependent values applicable to the entire material or the user may divide the material into regions and supply time-dependent temperatures for each region. The direct specification of fuel bearing material temperatures was applied here.

The direct specification of fuel bearing material temperatures was based on results from the AGR-1 thermal analysis, which was completed using the ABAQUS computer code.[4,5] Those results included the prediction of capsule-specific temperatures where each capsule was divided into approximately 25,000 finite element volumes. In general, the temperature predictions were made at four different times distributed through the planned irradiation of each capsule. In a post-processing step, capsule-specific minimum, volume-averaged, and maximum temperatures were determined for each of those times. Curve fits were then developed for minimum, volume-averaged, and maximum temperatures for Capsules 1 through 6 as shown in Figures 6 through 11. (It should be noted that the minimums and maximums are actually independent of the finite volume results because these were established by simply identifying the minimum and maximum temperature that occurred anywhere in each capsule at the time of each prediction.)

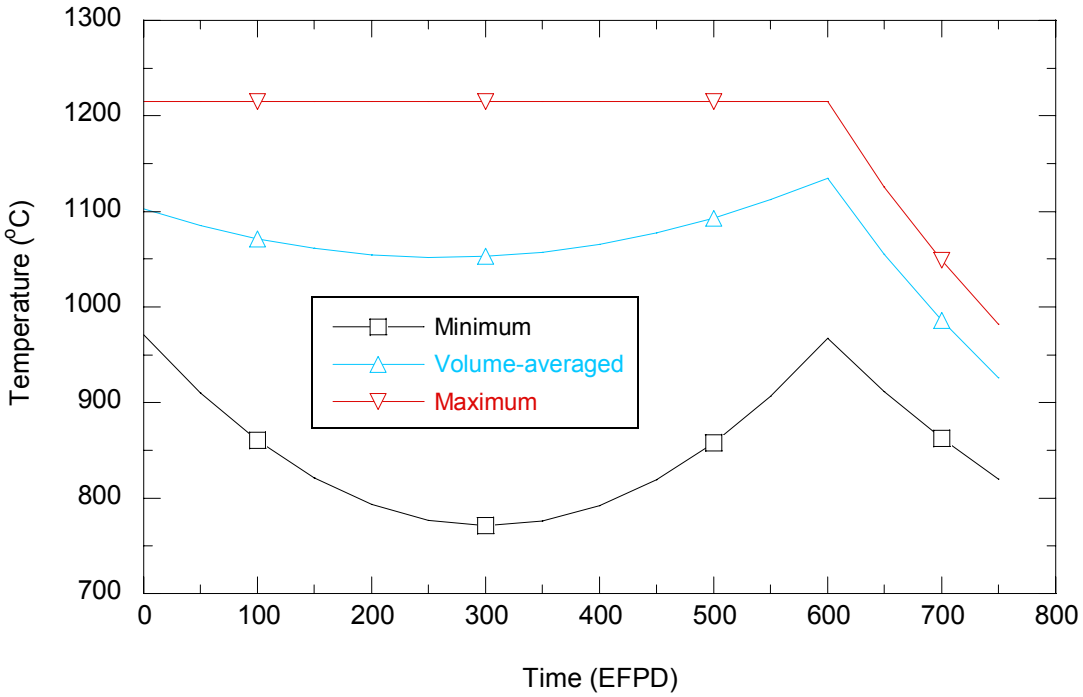

Figure 6. Capsule 1 temperatures as a function of time from AGR-1 thermal analyses.[4,5]

Two types of capsule-specific PARFUME calculations were completed with respect to these temperatures including (1) calculations with the entire capsule at a uniform time-dependent value and (2) calculations with capsule division and associated temperatures used directly from the thermal analysis. Specifically, calculations were made assuming each of the six capsules followed it's time-dependent volume average shown in Figures 6 through 11. Minimum and maximum temperatures for Capsule 3 (shown

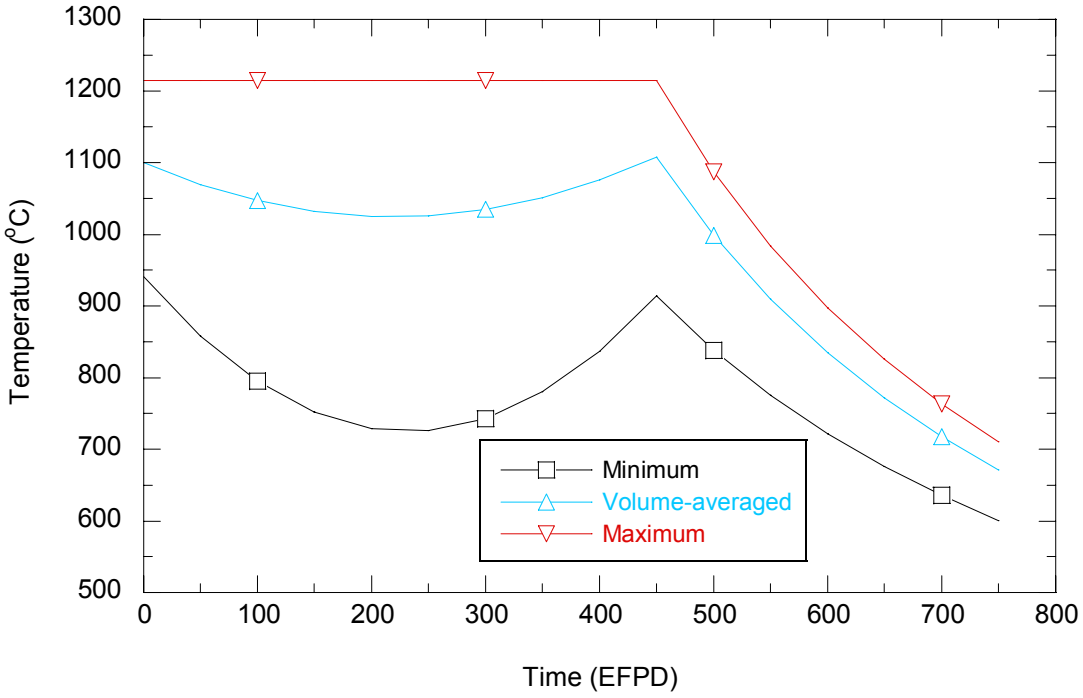

Figure 7. Capsule 2 temperatures as a function of time from AGR-1 thermal analyses.[4,5]

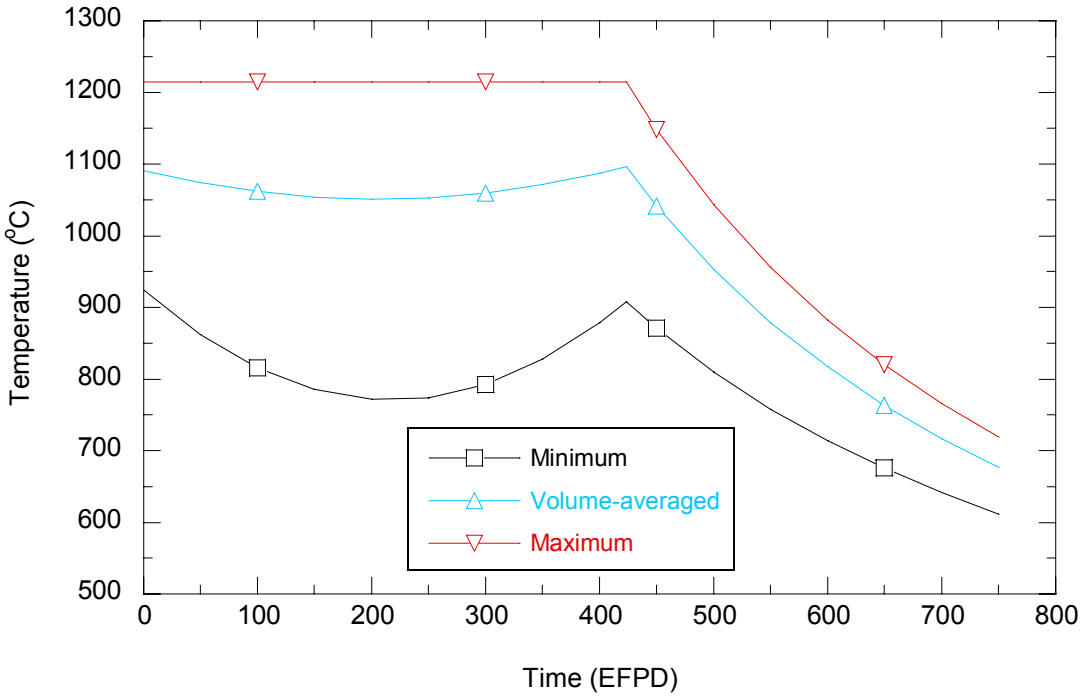

Figure 8. Capsule 3 temperatures as a function of time from AGR-1 thermal analyses.[4,5]

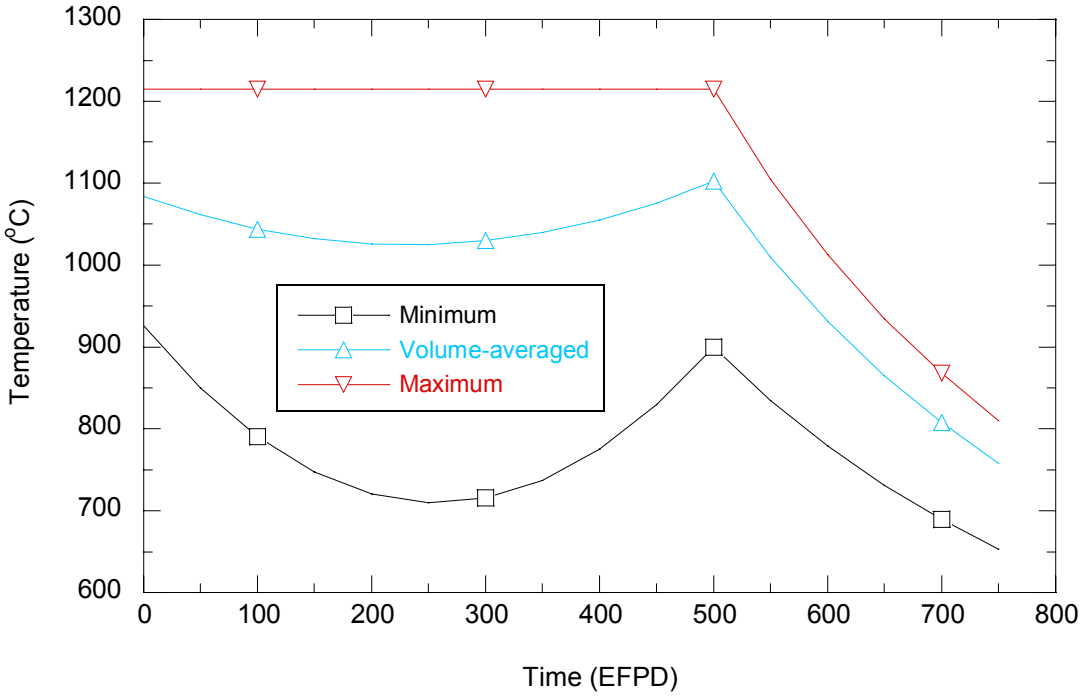

Figure 9. Capsule 4 temperatures as a function of time from AGR-1 thermal analyses.[4,5]

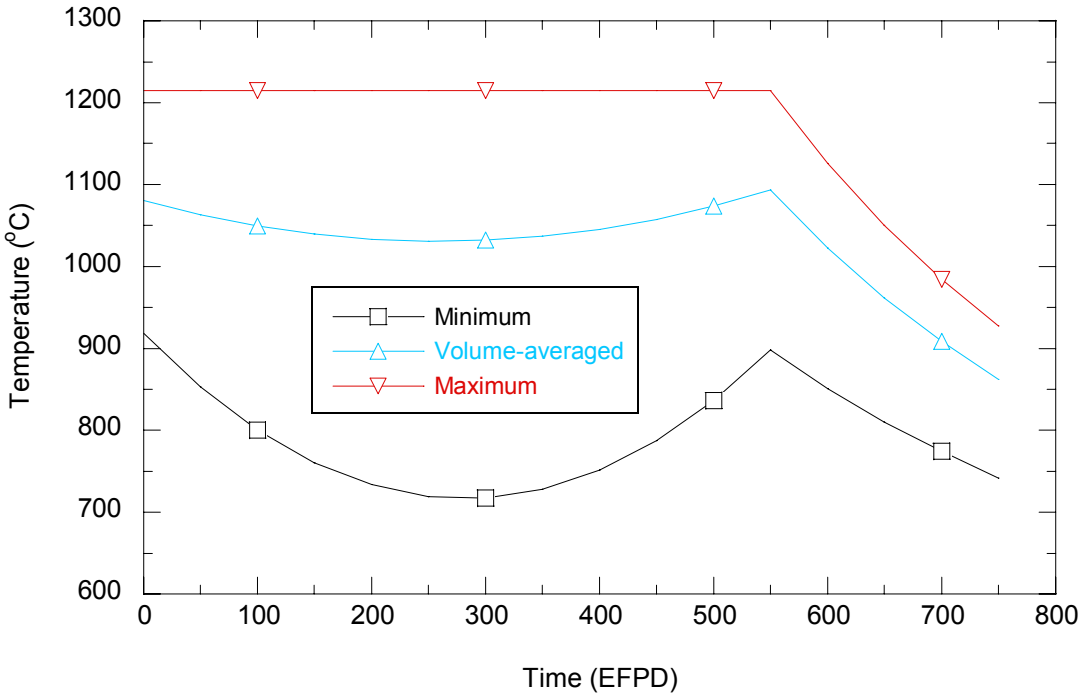

Figure 10. Capsule 5 temperatures as a function of time from AGR-1 thermal analyses.[4,5]

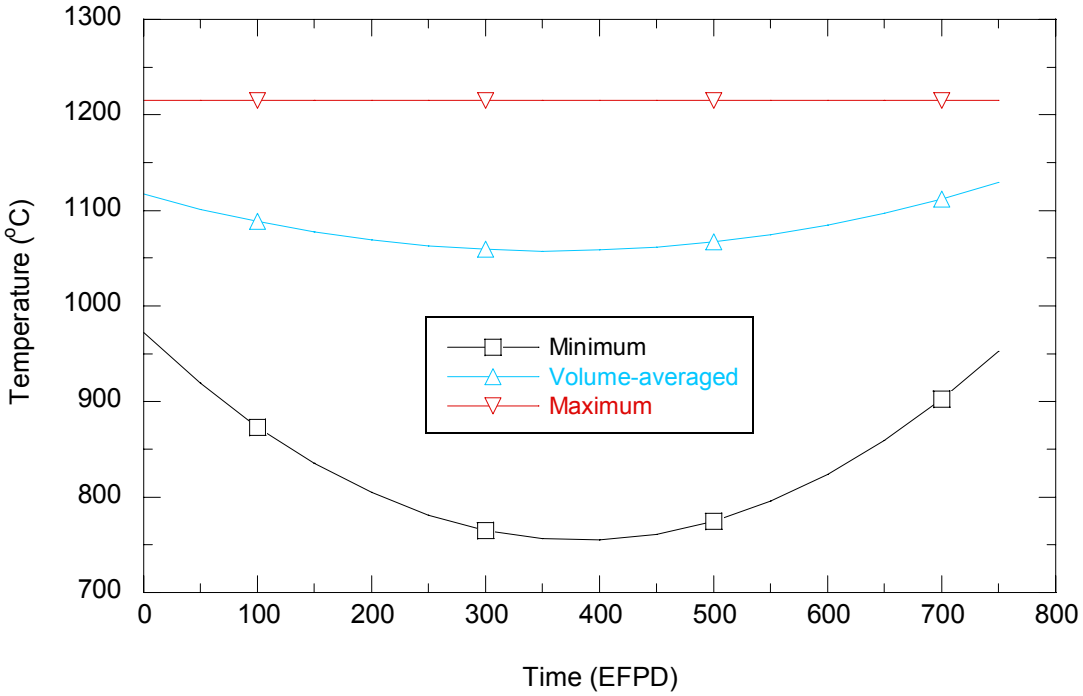

Figure 11. Capsule 6 temperatures as a function of time from AGR-1 thermal analyses.[4,5]

in Figure 8) were also considered separately. Note that all fuel particles (in a given capsule) share the same outer (OPyC) surface temperature in these eight calculations. In addition, a Capsule 3 calculation was made assuming division of the capsule into ~25,000 volumes with uniform time-dependent temperatures for each of those volumes consistent with the (ABAQUS) thermal analysis results. Binning was used to reduce the number of unique time-dependent temperatures to consider during analysis. Similar to all other calculations, OPyC outer surfaces were assumed to follow time-dependent temperatures representing each bin. This effectively provides a pseudo multi-dimensional thermal simulation within the otherwise one-dimensional PARFUME code. (Note that this code capability, although developed with ABAQUS in mind, will work equally well given appropriate inputs from other codes and/or actual measurements.)

The current practice for assigning OPyC outer surface temperatures yields particle temperature profiles that essentially "sit on top" of time-dependent capsule profiles, resulting in some over-prediction of particle temperatures. Although insignificant in these analyses, a potential for unrealistic kernel centerline temperatures exists, especially during accelerated irradiation. Consequently, a PARFUME refinement is being considered to link the effective volume-averaged capsule temperatures (from sources like ABAQUS) to a particle internal point (instead of the surface) to improve consistency with capsule results.

Note that the potential effects of an ATR high power (PALM) cycle were not considered in these analyses for two reasons. First, the AGR-1 irradiation will be complete before the next PALM cycle as currently planned for July 2009. Second, even if a PALM cycle occurs during the peak in AGR-1 fuel power generation (near 250 EFPD), it has been shown that the planned use of helium-3 as a PALM cycle sweep gas reduces power to an extent that targeted maximum fuel temperatures are not exceeded.[11] Therefore, the modeled temperatures (as outlined above) will bound those that could occur during a PALM cycle.

2.2. Input Parameters

PARFUME input parameters needed to model the AGR-1 test were taken from the Test Plan[2] and listed in Table 1. As indicated, a baseline fuel type and three other fuel variant types were included. Baseline fuel was used in Capsules 3 and 6, Variant 1 fuel was used in Capsule 5, Variant 2 fuel was used in Capsule 2, and Variant 3 fuel was used in Capsules 1 and 4.

Table 1. Parameters used in PARFUME modeling of the AGR-1 test.

Category	Parameter	Fuel Type[a] (mean value ± standard deviation)			
		Baseline	Variant 1	Variant 2	Variant 3
fuel characteristics	U235 enrichment (wt%)[b]	19.74			
	oxygen to uranium atom ratio[b]	1.361			
	carbon to uranium atom ratio[b]	0.3253			
	heavy metal contamination fraction[b]	1.0e-5			
geometry	kernel diameter (μm)	349.7 ± 9.0			
	buffer thickness (μm)	103.5 ± 8.2	102.5 ± 7.1	102.9 ± 7.3	104.2 ± 7.8
	IPyC thickness (μm)	39.4 ± 2.3	40.5 ± 2.4	40.1 ± 2.8	38.8 ± 2.1
	SiC thickness (μm)	35.3 ± 1.3	35.7 ± 1.2	35.0 ± 1.0	35.9 ± 2.1
	OPyC thickness (μm)	41.0 ± 2.1	41.1 ± 2.4	39.8 ± 2.1	39.3 ± 2.1
	particle asphericity[c]	1.13	1.132	1.129	1.127
material properties[d]	IPyC Weibull modulus[b]	9.5			
	SiC Weibull modulus[b]	6.0			
	OPyC Weibull modulus[b]	9.5			
	IPyC / SiC bond strength (MPa)[e]	100.0			
	PyC Poisson's ratio in creep[b]	0.5			
	PyC creep coefficient amplifier[e]	2.0			
	kernel density (g/cm^3)[b]	10.92			
	buffer density (g/cm^3)[b]	1.1			
	IPyC density (g/cm^3)[e]	1.904	1.853	1.912	1.904
	OPyC density (g/cm^3)[e]	1.907	1.898	1.901	1.911
	IPyC (post compact anneal) BAF[e]	1.033	1.021	1.036	1.034
	OPyC (post compact anneal) BAF[e]	1.033	1.03	1.029	1.036
boundary conditions[f]	ambient pressure (MPa)[b]	0.1			

a. Baseline fuel was used in Capsules 3 and 6, Variant 1 fuel was used in Capsule 5, Variant 2 fuel was used in Capsule 2, and Variant 3 fuel was used in Capsules 1 and 4.
b. Parameter standard deviation is not considered in PARFUME.
c. The mean value plus four standard deviations was conservatively used.
d. Values for properties that are not listed were based on data from Reference 12.
e. Parameter standard deviation was not part of the PARFUME model.
f. As discussed in Section 2.1, boundary conditions also include results from nuclear physics[3] and thermal analyses.[4,5]

As indicated in Table 1, statistical variations were considered relative to fuel particle geometry only (i.e., the kernel diameter, buffer thickness, IPyC thickness, SiC thickness, and the OPyC thickness). PARFUME also has the capability to address statistical variations in creep, bond strength, asphericity, IPyC density, OPyC density, IPyC Bacon anisotropy factor (BAF), and the OPyC BAF. With the exception of creep and bond strength, the AGR-1 Test Plan provides information regarding those variations. However, results from sensitivity calculations as listed in Table 2 indicate that those variations (which are small by specification) have little impact on the probability of AGR-1 fuel particle failures. For example, statistical variations in the IPyC BAF could increase the probability of fuel particle failure by only 0.1284% relative to the number of failures associated with fuel particle geometry variations alone. Similarly, statistical variations in the IPyC density could decrease the probability of fuel particle failure by only 0.2760%. Because the effects are so small, statistical variations in asphericity, IPyC density, OPyC density, IPyC BAF, and the OPyC BAF were not considered. (Nevertheless, note that asphericity for all fuel types was conservatively set at four standard deviations above the mean value for consistency with Revision 0 of this EDF.)

Table 2. Results from sensitivity calculations to evaluate the impact of fuel statistical variations.[a]

Fuel Variation[b]	% Difference[c] in the Probability of						
		Failure due to					
	Failure	Amoeba	IPyC Cracking	IPyC Debonding	Pressure	IPyC Cracking	IPyC Debonding
IPyC BAF	0.1284	0	0.1284	0	0	0.0304	0
OPyC BAF	-0.0168	0	-0.0168	0	0	-0.0190	0
IPyC density	-0.2760	0	-0.2760	0	0	-0.2815	0
OPyC density	-0.0252	0	-0.0252	0	0	-0.0038	0
Asphericity	-0.0048	0	-0.0048	0	0	-0.0038	0

a. Using 2-loop integration with baseline fuel characteristics.
b. In addition to variations in the dimensions of the five fuel particle materials.
c. Relative to results associated with variations in the dimensions of the five fuel particle materials only.

It should be noted that results listed in Table 2 were generated using the 2-loop integration scheme. To ensure that those results were not adversely affected by simplifications inherent in 2-loop integration, sensitivity calculations were completed as listed in Table 3 to compare full-loop integration results with results from the simplified (2- and 3-loop) schemes. As indicated, both 2-loop and 3-loop integration results (obtained with substantial savings in run time) agree very closely with full-loop integration. (A description of the integration algorithm is given in Reference 13.) Consequently, Table 2 results are completely acceptable for discounting the need for treating the identified statistical fuel particle variations. Table 3 results are also notable on their own merit in demonstrating that the three integration schemes are correctly implemented in PARFUME.

2.3. Multi-Dimensional Stress

In addition to the one-dimensional behavior of a symmetrical spherical fuel particle, PARFUME considers multi-dimensional behavior including 1) an aspherical geometry, 2) cracking of the IPyC layer, and 3) partial debonding of the IPyC from the SiC. To model such effects, PARFUME utilizes the results of

Table 3. Results from sensitivity calculations to evaluate the impact of various solution schemes.[a]

Integration Scheme	% Difference in the Probability of							% Difference in Run Time
		Failure due to						
	Failure	Amoeba	IPyC Cracking	IPyC Debonding	Pressure	IPyC Cracking	IPyC Debonding	
3 loop	-0.0012	0	-0.0012	0	0	0	0	-86.46
2 loop	-0.0156	0	-0.0156	0	0	0	0	-98.61

a. Relative to results obtained using full-loop integration with baseline fuel characteristics.

detailed finite element analyses for cracked, debonded, and/or aspherical particles in conjunction with results from the PARFUME closed form one-dimensional solution to make a statistical approximation of the stress levels in any particle.[14,15] Version 6.4-1 of ABAQUS[16] was used to perform the finite element stress analyses to capture the multi-dimensional effects. The corresponding statistical parameters as used here are listed in Table 4. (ABAQUS Version 6.4-1 has satisfied INL V&V requirements under Tracking Number 125097.[17])

2.4. Material Properties

Material properties used in PARFUME are generally obtained from Reference 12. As such, the elastic moduli and swelling strains for the IPyC and OPyC are treated as functions of fluence. The effective range for these properties extends to a fluence of 3.96e25 n/m^2. However, an approximation was necessary to enable PARFUME modeling of some capsules in the AGR-1 test where the end-of-life fluence reaches as much as 4.53e25 n/m^2. The approximation consists of treating the elastic moduli and swelling strain rates as constants in PARFUME beyond a fluence level of 3.96e25 n/m^2.

The historical creep coefficient for the pyrocarbons layers[12] was found to be significantly lower than what has been used in other fuel performance models. It has also been found that PARFUME gives favorable comparisons with results of the New Production - Modular High Temperature Gas Reactor (NP-MHTGR) experiments if the historical creep coefficient is approximately doubled.[14] Therefore, the creep coefficient used in predictions for the AGR-1 test was set equal to twice the historical value.

As discussed in Reference 18, there is significant uncertainty in how well the physical properties of the coating layers are known. The accuracy of failure probability predictions from any fuel performance code relies on the accuracy of these properties.

2.5. Physico-Chemical Behavior

The internal gas pressure is calculated in PARFUME as a function of time according to the Redlich-Kwong equation of state.[19] Parameters utilized in this equation are derived from the critical temperature and pressure of each gas specie occupying the void volume within the particle.[20] PARFUME considers the generation of CO and the release of the noble gas fission products, xenon and krypton, in this pressure calculation.

Table 4. Statistical parameters used in PARFUME modeling of the AGR-1 test.

Correlation Coefficients for IPyC Cracking[a]			
Coefficient		C1[b]	C2[b]
for IPyC thickness		1.38458E-02	-6.61658E-05
for SiC thickness		9.23202E-03	3.06423E-04
for OPyC thickness		-1.70276E-02	3.42208E-04

Correlation Coefficients for Asphericity[a]			
Coefficient		C1[c]	C2[c]
for Asphericity effects	Function h_{11}	5.37926	-82.1235
	Function h_{21}	6.83819	-94.0798

SiC Strength and Stress for IPyC Cracking		
Capsule	σ_{ms} (MPa)[d]	$\sigma_{c\bar{v}}$ (MPa)[e]
1	1119.98	177.197
2	1122.95	195.051
3 (high temperature)	1123.32	145.628
3 (volume averaged temperature)	1123.34	181.578
3 (low temperature)	1123.59	277.524
4	1120.0	183.15
5	1120.22	193.748
6	1123.22	176.987

SiC Strength and Stress for Asphericity			
Capsule	σ_{ms} (MPa)[f]	$\sigma_{c\bar{v}}$ (MPa)[g]	$\Delta\sigma_{c\bar{v}}$ (MPa)[g]
all	529.338	425.933	340.677

a. Representing averages for all six capsules.
b. Equations 6 and 8 of Reference 14.
c. Equations 2 and 8 of Reference 15.
d. Equation 15 of Reference 14.
e. Equation 8 of Reference 14.
f. Equation 4 of Reference 15.
g. Equation 8 of Reference 15.

CO production is calculated in PARFUME using an algorithm derived from thermochemical free energy minimization calculations performed by the HSC computer code.[21] Input to the HSC code in developing this algorithm consisted of elemental fission product inventories generated by the MOCUP computer code,[22] which couples the MCNP and ORIGEN2 computer codes.[23,24] This CO production model considers burnup, temperature, uranium enrichment, and fuel composition in the calculation.

PARFUME calculates fission product gas release due to both recoil and diffusion. Direct fission recoil from the kernel to the buffer is accounted for by geometrical considerations and fission fragment ranges derived from compiled experimental data.[25] Diffusive release is calculated according to the Booth equiva-

lent sphere diffusion model,[26] which utilizes an effective diffusion coefficient formulated by Turnbull.[27] This effective diffusion coefficient accounts for intrinsic, thermal, and irradiation-enhanced diffusion.

A model accounting for release of short-lived fission product gases from failed particles and from uranium contamination in the fuel bearing material is incorporated into PARFUME. This model calculates release rate to birth rate (R/B) ratios for several prominent fission product nuclides. Also, based upon the Booth equivalent sphere gas release model,[28] this model uses different reduced diffusion coefficients for release from failed particles[29] and from uranium contamination.[30]

2.6. Failure Mechanisms Considered

Four potential failure mechanisms are currently considered in PARFUME. The first is a pressure vessel failure caused by the buildup of fission gases. Stresses for this failure mechanism are determined using the one-dimensional solution in PARFUME for a three-layer (IPyC-SiC-OPyC) particle. Because of asphericity in the particle shape, these stresses are modified based on results of finite element analysis of aspherical particles. Stress modification was based on Table 4 coefficients in this EDF. However, particle internal pressures were found to be too low to trigger this failure mechanism in AGR-1 test calculations.

The second mechanism considered is failure of the SiC layer caused by partial debonding of the IPyC from the SiC. Debonding, if it occurs, results from IPyC shrinking inward away from the SiC during irradiation. PARFUME first determines whether debonding between the layers occurs by comparing the radial stress between layers with the bond strength between layers. If debonding is determined to occur, then the code estimates the stress in the SiC layer accounting for multidimensional effects using a previously documented methodology.[14,15] Because AGR-1 particle fabrication was based on German processes, the bond strength was set at a value that is considered to be representative for German particles (i.e., 100 MPa). At this bond strength, IPyC / SiC debonding was not predicted, and therefore debonding did not contribute to particle failures in the AGR-1 test.

The third failure mechanism considered in PARFUME is migration of the fuel kernel into the SiC layer, or the amoeba effect. This failure mechanism has the potential to occur if the particles are subjected to a global temperature gradient. However, the amoeba effect made no contribution to particle failures in these analyses because migration coefficients for UCO fuels are very small.

The fourth and final failure mechanism currently considered in PARFUME is failure of the SiC layer caused by irradiation-induced shrinkage and the associated cracking of the IPyC layer. The presence of a crack in the IPyC layer creates a stress concentration in the SiC layer.[31] To treat the multi-dimensional effects of this stress concentration, PARFUME estimates stresses in the SiC layer resulting from the presence of a crack based on a previously documented methodology.[14,15] Table 4 contains coefficients used to apply that methodology in the AGR-1 test. In evaluating failures due to IPyC cracking, PARFUME first determines whether the IPyC layer cracks using the Weibull statistical theory. If the IPyC layer is predicted to crack, the particle is evaluated for failure of the SiC layer due to the presence of the crack. All fuel particle failures in AGR-1 test calculations were found to be due to this mechanism.

Chemical attack of the SiC (primarily) by Pd represents another potential failure mechanism. Although PARFUME does not currently simulate this mechanism, scoping calculations have shown that fuel particle failure occurs when penetration through the thickness of the SiC is complete,[32] leading to the direct release of fission products. Based on Pd penetration rates,[33] however, SiC failure would not occur in the AGR-1

test even if particle temperatures were assumed to remain fixed at the maximum calculated value for the entire irradiation period.

PARFUME uses the Weibull statistical theory to determine whether particles fail, using a mean strength for the SiC layer based on a stress distribution corresponding to the failure mechanism under consideration. The failure modes are implemented such that a particle fails only in the mode of failure that would occur first for that particle. The code retains the time at which failures occur, allowing for the construction of a time evolution of the failure probability for a batch of fuel particles. Weibull parameters used to evaluate failures of the SiC layer and cracking of the IPyC layer were obtained from Reference 12.

3. RESULTS

Analyses of the AGR-1 test were completed based on PARFUME modeling as discussed above. Corresponding results from those analyses are summarized in Tables 5 and 6.

Table 5. Results after 750 days of irradiation based on capsule-specific volume-averaged temperatures.[a]

Capsule	Fuel Type	EOL Fluence (10^{25} n/m^2 @ E > 0.18 MeV)	Probability of							Number of failed particles / capsule[b]
			Failure	Failure due to				IPyC Cracking	IPyC Debonding	
				Amoeba	IPyC Cracking	IPyC Debonding	Pressure			
1	Variant 3	3.501	5.6e-7	0	5.6e-7	0	0	3.0e-2	0	< 1
2	Variant 2	4.310	1.5e-6	0	1.5e-6	0	0	4.2e-2	0	< 1
3	Baseline	4.526	7.1e-7	0	7.1e-7	0	0	3.3e-2	0	< 1
4	Variant 3	4.524	9.1e-7	0	9.1e-7	0	0	3.9e-2	0	< 1
5	Variant 1	4.058	1.7e-6	0	1.7e-6	0	0	5.2e-2	0	< 1
6	Baseline	3.139	4.8e-7	0	4.8e-7	0	0	2.6e-2	0	< 1

a. Using full-loop integration.
b. Assuming outer surfaces of all fuel particles are at capsule-specific volume-averaged temperatures.

Table 6. Capsule 3 results after 750 days of irradiation for various capsule temperatures.[a]

Capsule Temperature	Probability of							Number of failed particles / capsule[b]
	Failure	Failure due to				IPyC Cracking	IPyC Debonding	
		Amoeba	IPyC Cracking	IPyC Debonding	Pressure			
Low	1.9e-4	0	1.9e-4	0	0	7.2e-1	0	9
ABAQUS data[c]	1.5e-6	0	1.5e-6	0	0	4.1e-2	0	< 1
Volume-averaged	7.1e-7	0	7.1e-7	0	0	3.3e-2	0	< 1
High	2.9e-8	0	2.9e-8	0	0	5.1e-3	0	< 1

a. Full-loop integration was used in all calculations except the 'ABAQUS data' run where 2-loop integration was used
b. Assuming outer surfaces of all fuel particles in the capsule are at the specified temperatures.
c. Best estimate.

Results in Table 5 were generated assuming the outer surfaces of all fuel particles in each capsule are at capsule-specific volume-averaged temperatures as shown in Figures 6 through 11. As indicated in the table, IPyC cracking is the only mechanism leading to fuel particle failures under those conditions and the calculated fuel particle failure probabilities are low. Less than one fuel particle failure is predicted per capsule for all 6 capsules given the calculated failure probabilities.

Table 6 results provide a more detailed evaluation of the range of conditions that are possible in Capsule 3. Specifically, results were generated assuming the outer surfaces of all fuel particles in the capsule follow either low, volume-averaged, or high temperatures as shown in Figure 8. In addition, results are provided based on temperature distributions derived using ABAQUS data from the AGR-1 thermal analyses.[4,5] Like Table 5 results, all fuel particle failures are due to IPyC cracking, the probability of which increases as temperatures decrease. This trend develops because the temperature effect on irradiation-induced creep is larger than the temperature effect on irradiation-induced shrinkage. Consequently, as temperatures decrease, stress relief afforded by creep is diminished more than the reductions in stress buildup associated with shrinkage.

It should be noted that, with the exception of results based on ABAQUS data, the number of failed fuel particles per capsule as given in Tables 5 and 6 are only approximations. These are approximations because the compacts in each capsule will never be at any uniform temperature (as assumed in the calculations). Instead, fuel particles in each capsule will be exposed to some distribution of temperature. Consequently, the calculated number of fuel particle failures per capsule (as listed in the tables) strictly applies only if all fuel particles in the capsules are exposed to the assumed uniform temperatures, and will only be approximations otherwise.

The fact that capsule temperatures are not uniform is best modeled in the current version of PARFUME using ABAQUS data, where a user-defined number can be set to 'bin' particles having similar temperatures. The number of particles in each bin is easily determined and therefore, the probability of having a particle at any of the representative 'bin' temperatures can be established. Using this approach allows calculation of the actual number of fuel failures (within the standard limitations associated with application of any discrete numerical algorithm). Results shown in Table 6 indicate the best estimate of fuel particle failure probability for Capsule 3 is 1.5e-6, which corresponds with failure of less than one fuel particle in this capsule. This probability is somewhat higher than the probability (of 7.1e-7) derived from assuming that the outer surfaces of all particles follow the volume-averaged temperature shown in Figure 8. Note that if this trend holds for other capsules, failure probabilities based on volume-averaged temperatures as listed in Table 5 may be somewhat non-conservative.

With the exception of the 'ABAQUS data' run, Table 5 and 6 results were calculated using PARFUME full-loop integration. However, the 'ABAQUS data' run introduces an additional integration variable (to accommodate temperature binning) to the five particle geometry variables already considered (i.e., the kernel diameter and buffer, IPyC, SiC, and OPyC thicknesses). This temperature addition would significantly increase the run-time under full-loop integration. For that reason, 2-loop integration was used for the 'ABAQUS data' run. Table 7 calculations were completed to demonstrate that time-saving simplifications in 2-loop integration do not adversely affect results.

As indicated in Table 7, 'ABAQUS data' runs were performed using full-loop, 3-loop, and 2-loop integration while neglecting variations in kernel diameter and buffer thickness. Although full-loop integration represents the most accurate solution, it is clear that both 3-loop and 2-loop results are closely comparable to the full-loop results. In fact, the maximum discrepancy between 2-loop and full-loop results is only

Table 7. Results from Capsule 3 sensitivity calculations to evaluate the impact of various solution schemes when ABAQUS temperature data is used.[a]

Integration Scheme	Probability of							Number of Failed Particles	Run Time (s)
	Failure	Failure due to				IPyC Cracking	IPyC Debonding		
		Amoeba	IPyC Cracking	IPyC Debonding	Pressure				
Full-loop	1.4991e-6	0	1.4991e-6	0	0	4.0296e-2	0	< 1	113
3-loop	1.4990e-6	0	1.4990e-6	0	0	4.0288e-2	0	< 1	69.5
2-loop	1.4958e-6	0	1.4958e-6	0	0	4.0286e-2	0	< 1	19.4

a. Without variations in kernel diameter and buffer thickness.

0.2% in spite of run time reduction by a factor of ~6. This indicates that Table 6 results can be directly compared regardless of solution methods applied. Furthermore, Table 7 results are a notable demonstration that all three integration techniques are working properly given temperature data input.

The remainder of this section contains a description of predicted events and conditions leading to the results just described. This discussion is offered as a way to provide further insights into the AGR-1 test.

Irradiation can lead to the development of a gap between the buffer and the IPyC. The gap can develop as a result of the combined effects of kernel swelling; shrinkage and creep in the buffer, IPyC, and OPyC layers; the effects of particle internal pressure, and the kernel/buffer contact pressure. However, differences in density between the buffer and the IPyC is a primary factor in the process. The buffer, which is much more porous than the dense IPyC layer, shrinks more during irradiation. The growth rate for the gap size slows, however, as the buffer becomes more dense during irradiation. The size of this gap is shown in Figure 12 for nominal particles assuming outer surfaces of those particles follow capsule-specific volume-averaged temperatures. Inspection of this figure indicates that gap width is closely correlated with fluence, which in turn is correlated with the axial position of the capsules in the ATR core. Because ATR operates with a cosine-like profile, gap widths tend to be smallest in the outermost capsules (numbered 1 and 6 that are exposed to relatively low fluence levels) and largest in capsules at the core midplane (numbered 3 and 4 that are exposed to relatively high fluence levels).

Comparisons of the gap width as a function of temperature are shown in Figure 13. The gap width tends to increase with temperature as indicated because irradiation-induced shrinkage is temperature-dependent.

The buffer-to-IPyC gap can be a significant fraction of the thermal resistance in a fuel particle. Consequently, if other conditions are equal, temperature differentials (from the kernel centerline to the outer surface of the OPyC) are higher across particles with larger gaps. This trend is apparent in Figure 14, where temperature differentials are shown assuming the outer surfaces of particles follow volume-averaged temperatures. In these figures, temperature differentials are higher in Capsule 3 and 4 particles than in Capsule 1 and 6 particles, which would be expected given capsule-to-capsule differences in the buffer-to-IPyC gaps (shown in Figures 13). (For reference, kernel centerline temperatures for all six capsules at volume-averaged temperatures and for Capsule 3 at various temperatures are shown in Figures 15 and 16, respectively. The segmented appearance of the 'ABAQUS temperature' curve in Figure 16 is due to limitations in the number of available ABAQUS results.)

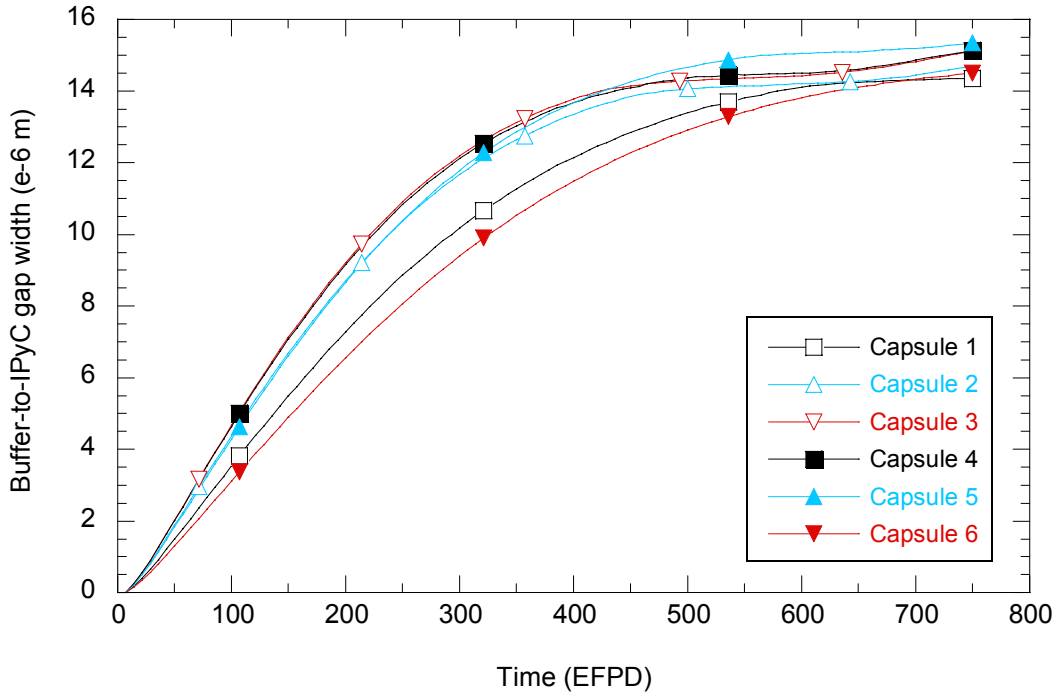

Figure 12. Buffer-to-IPyC gap width in nominal particles assuming volume-averaged capsule temperatures.

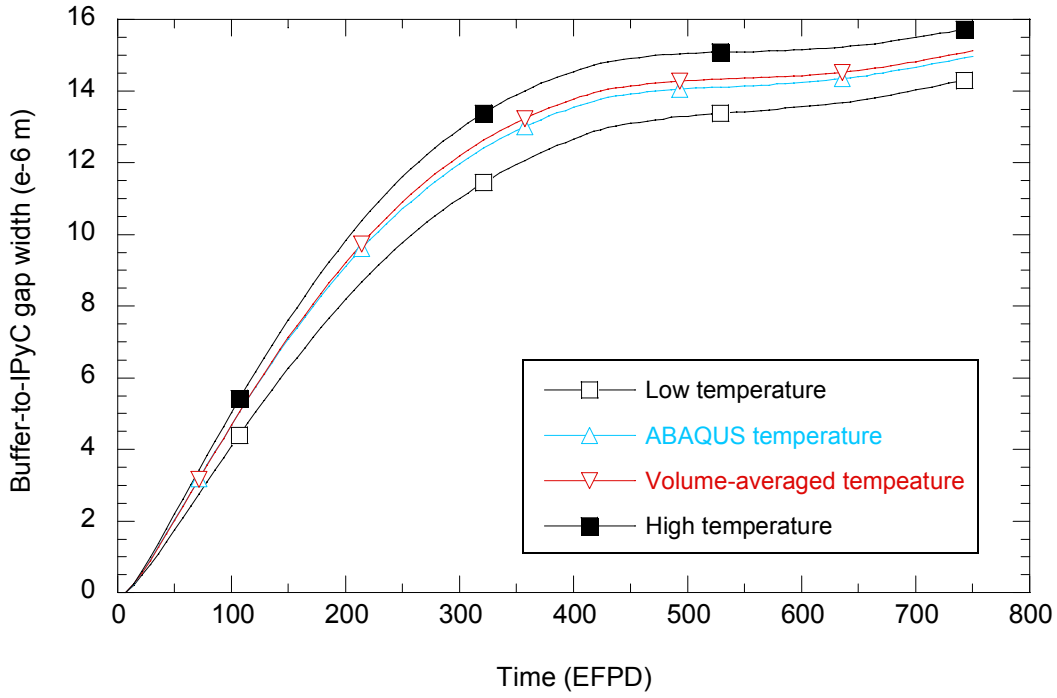

Figure 13. Buffer-to-IPyC gap widths in Capsule 3 nominal particles for various capsule temperatures.

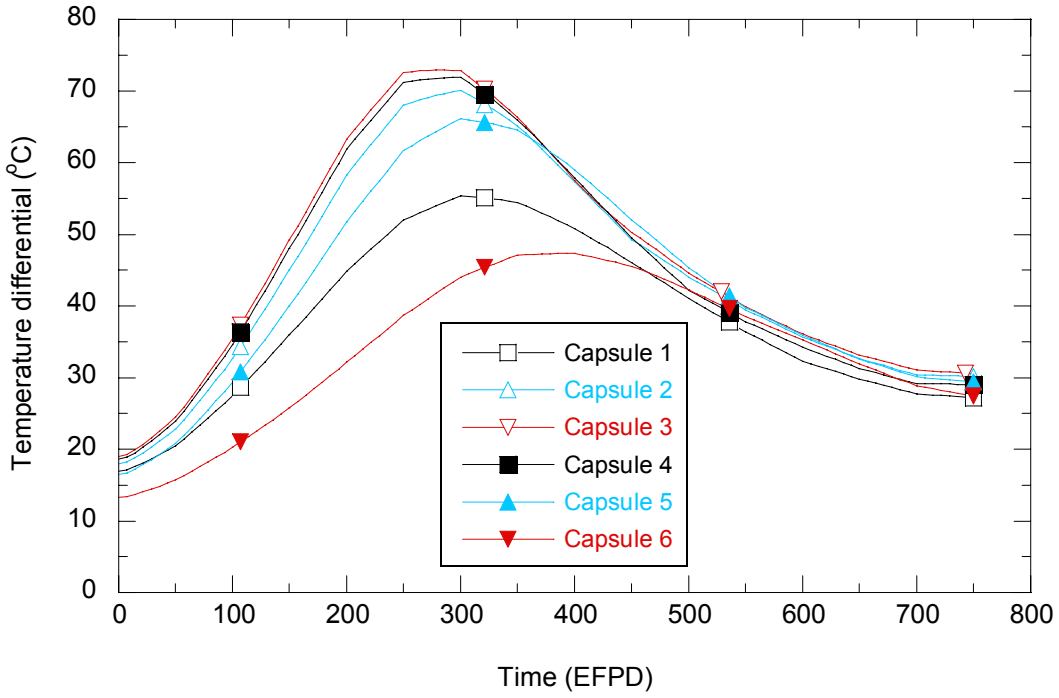

Figure 14. Particle temperature differentials (from the kernel centerline to the outer surface of the OPyC) assuming volume-averaged capsule temperatures.

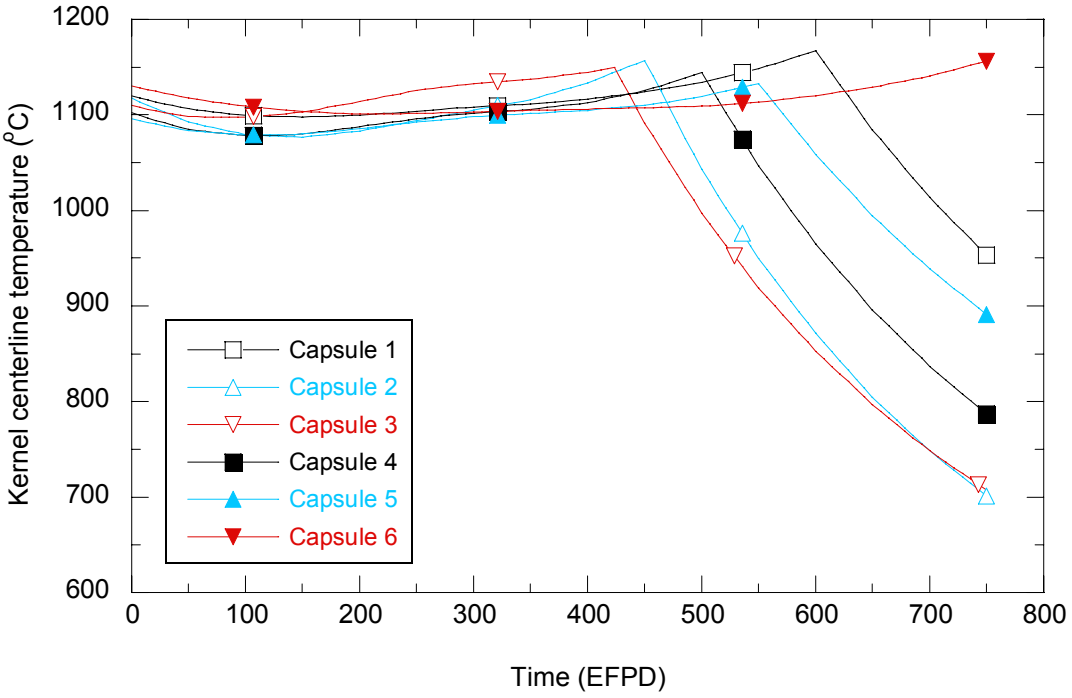

Figure 15. Kernel centerline temperatures assuming volume-averaged capsule temperatures.

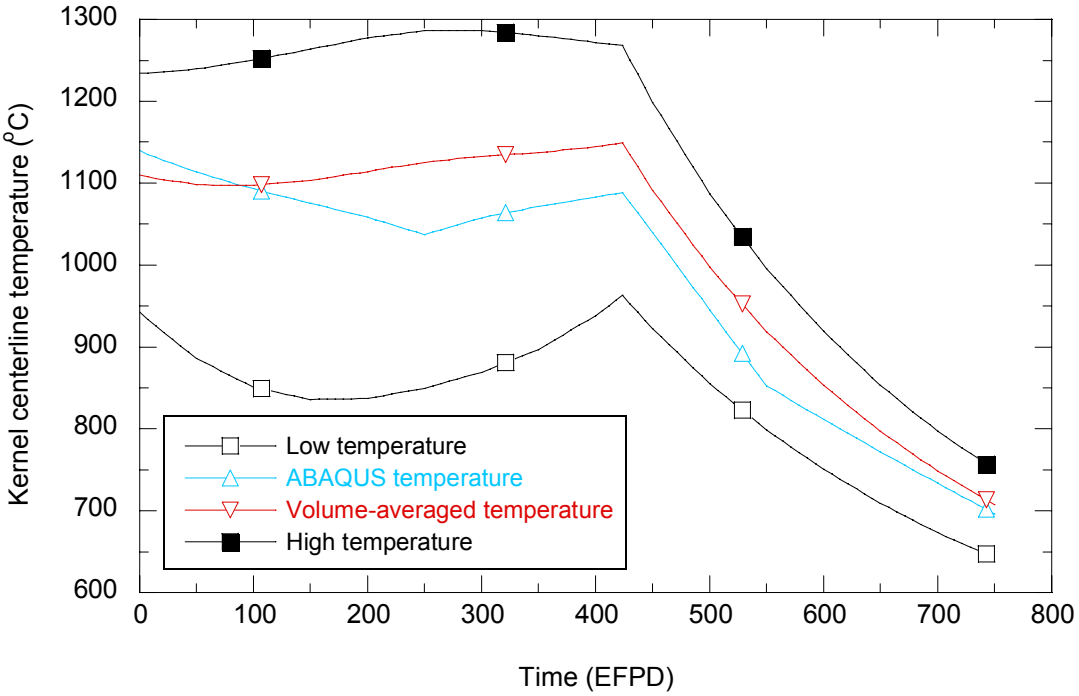

Figure 16. Capsule 3 kernel centerline temperatures for various capsule temperatures.

Particle internal pressures tend to increase as temperatures increase. This occurs because fission product release and the pressure of confined gases both increase with temperature. This trend is apparent in Figure 17 where Capsule 3 fuel particles with the hottest temperatures reach the highest internal pressures. Internal pressures for particles in all capsules exposed to volume-averaged temperatures are shown in Figure 18 for reference.

SiC inner tangential stresses for Capsule 3 particles exposed to various temperatures are shown in Figure 19 (in regions well removed from any cracks in the IPyC). As indicated, stresses decrease as temperatures increase. Although internal pressures, shrinkage, creep, and thermal effects all contribute to the stress in a particle, the stress magnitude decreases as temperatures increase because higher pyrocarbon creep at higher temperature more than offsets the increased shrinkage. For this reason, stress magnitudes in hotter particles tend to be less than those in cooler particles. Capsule-to-capsule comparisons of SiC inner tangential stresses are shown in Figure 20.

Ultimately, particle failures are directly related to particle stresses. Calculated failure probabilities for all capsules at volume-averaged temperatures are presented in Figure 21. Capsule 3 failure probabilities are shown in Figure 22 for various capsule temperatures. Because shrinkage of the pyrocarbons has the greatest effect relatively early during irradiation, failure probabilities driven by shrinkage-induced IPyC cracking peak well before the fluence has reached 1.e25 n/m^2. (Corresponding probabilities for IPyC cracking are shown in Figures 23 and 24.)

Given that less than one fuel particle failure is predicted in each capsule evaluated (assuming capsule-specific volume-averaged temperatures), fission product release will be very small and determined only by the amount of uranium contamination. Release/birth (R/B) results presented in Figures 25 through 27 are

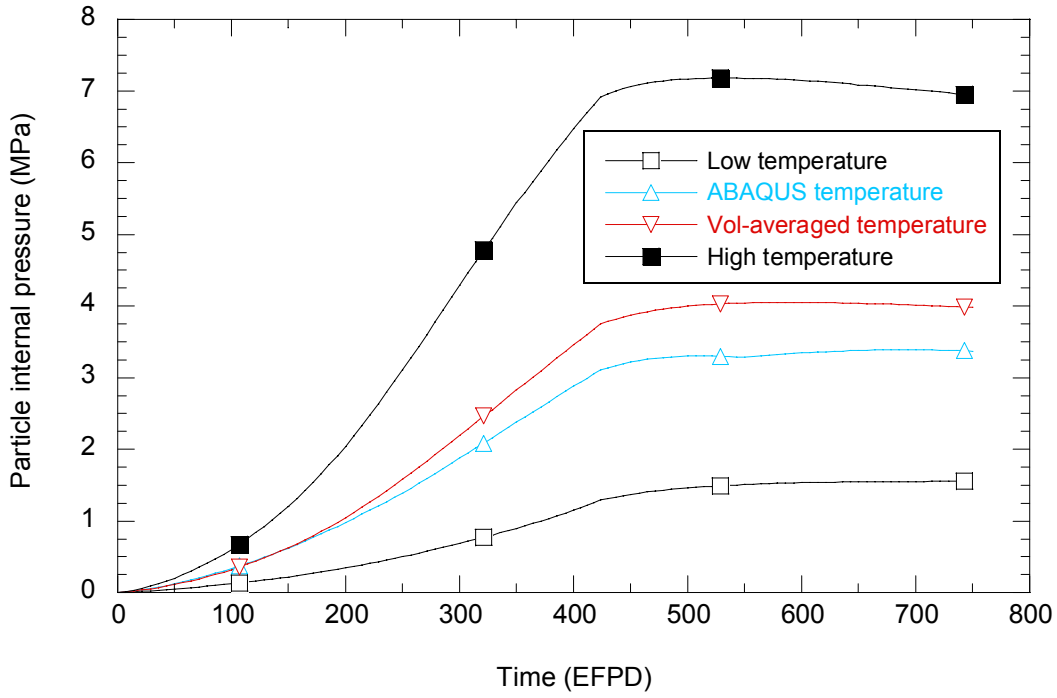

Figure 17. Capsule 3 particle internal pressures for various capsule temperatures.

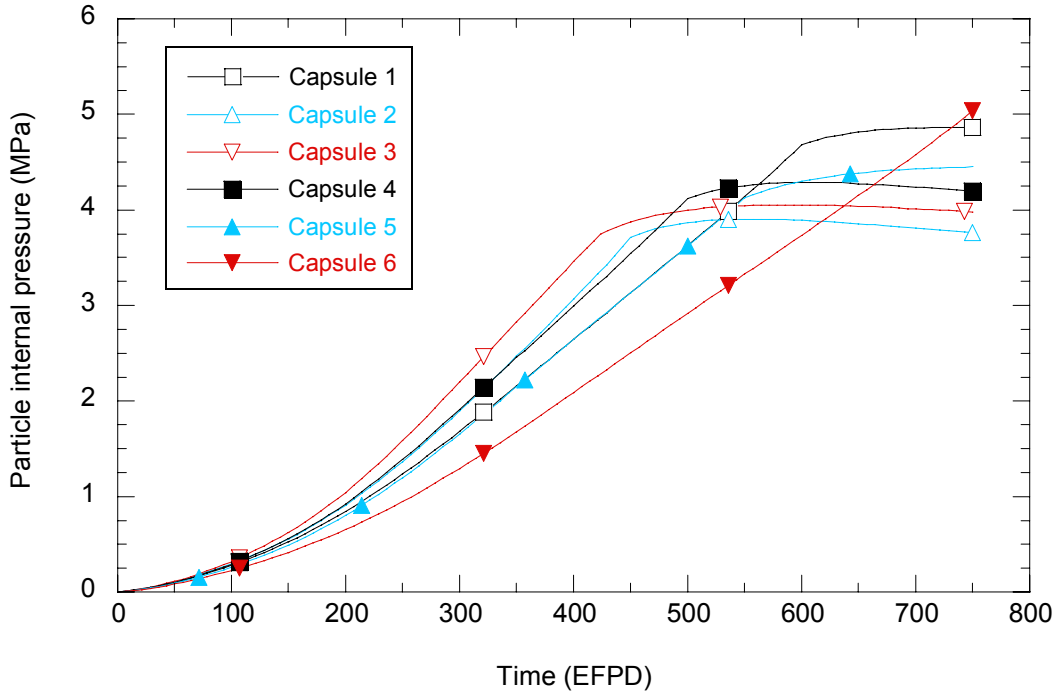

Figure 18. Particle internal pressures assuming volume-averaged capsule temperatures.

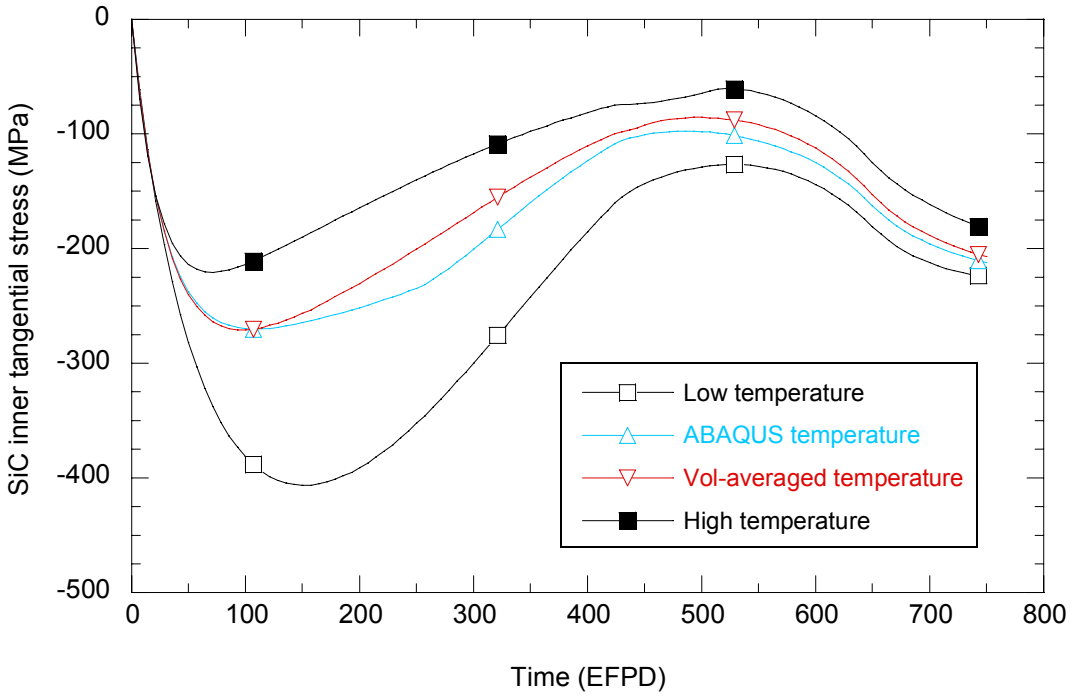

Figure 19. Capsule 3 SiC inner tangential stress for various capsule temperatures.

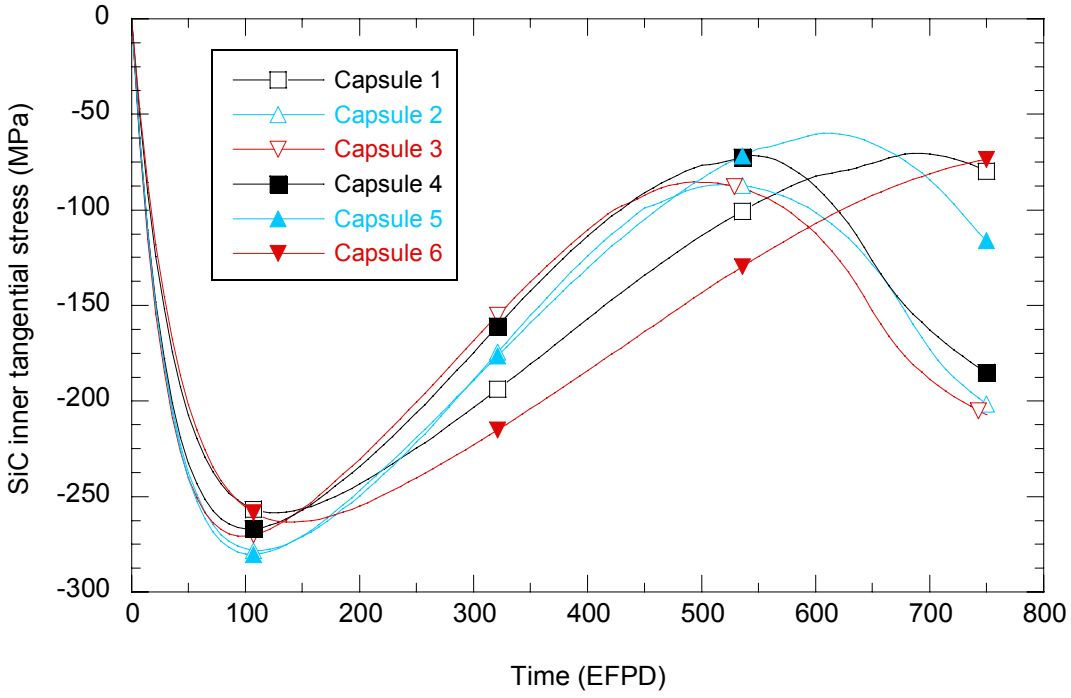

Figure 20. SiC inner tangential stress assuming volume-averaged capsule temperatures.

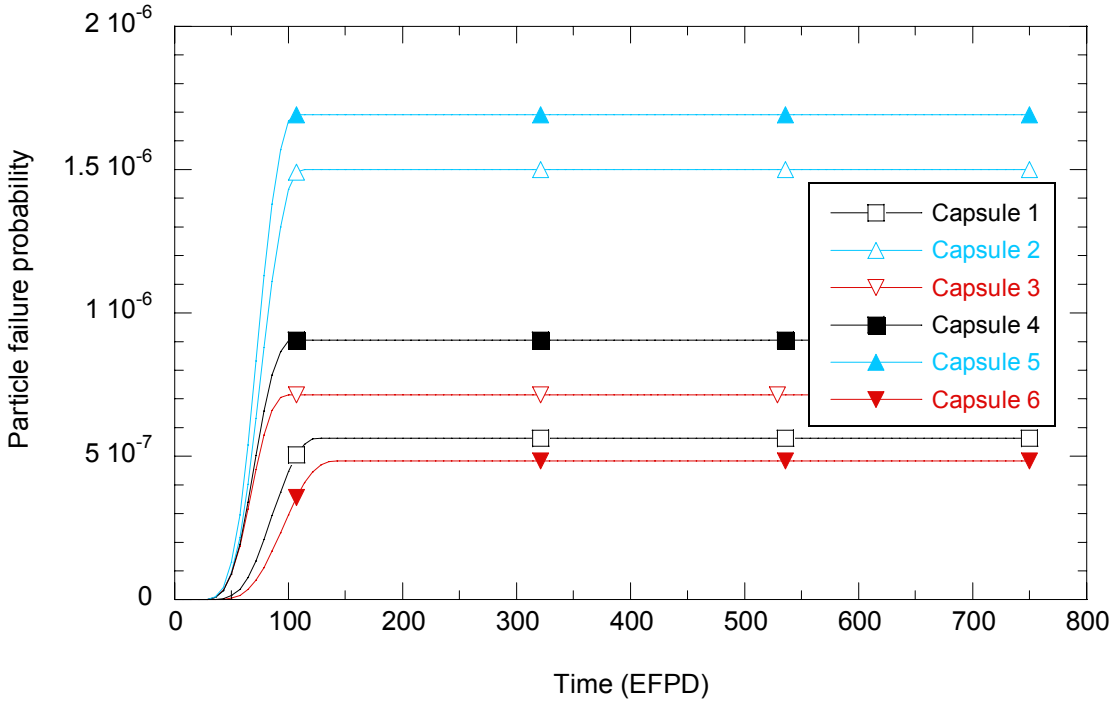

Figure 21. Fuel particle failure probabilities assuming volume-averaged capsule temperatures.

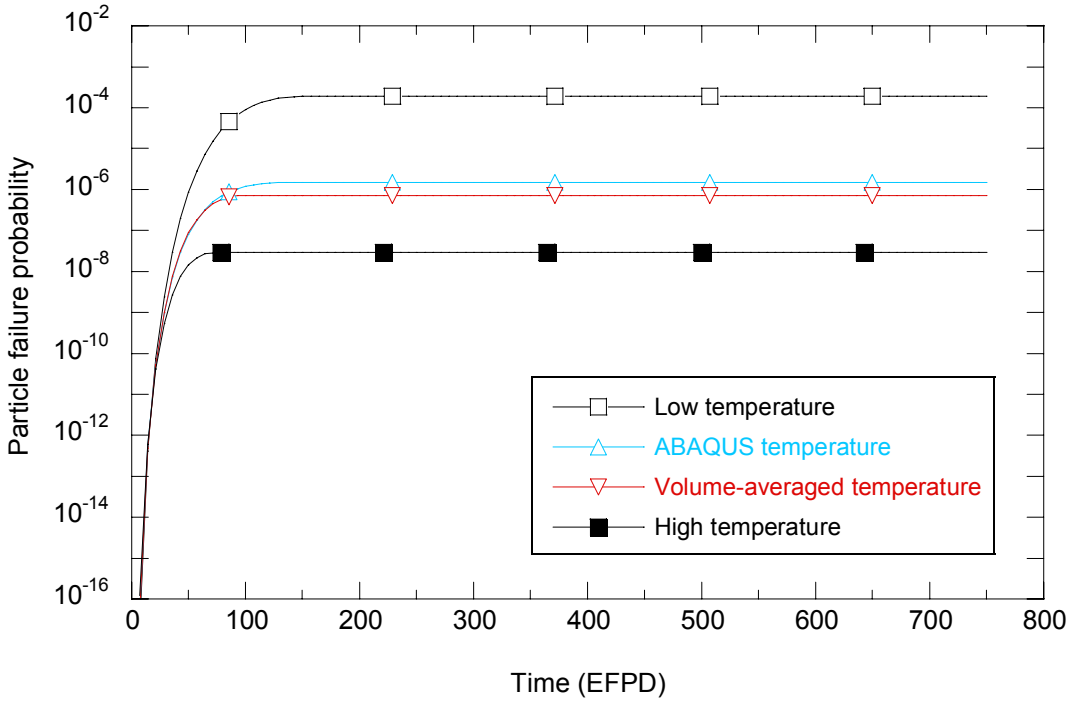

Figure 22. Capsule 3 fuel particle failure probabilities for various capsule temperatures.

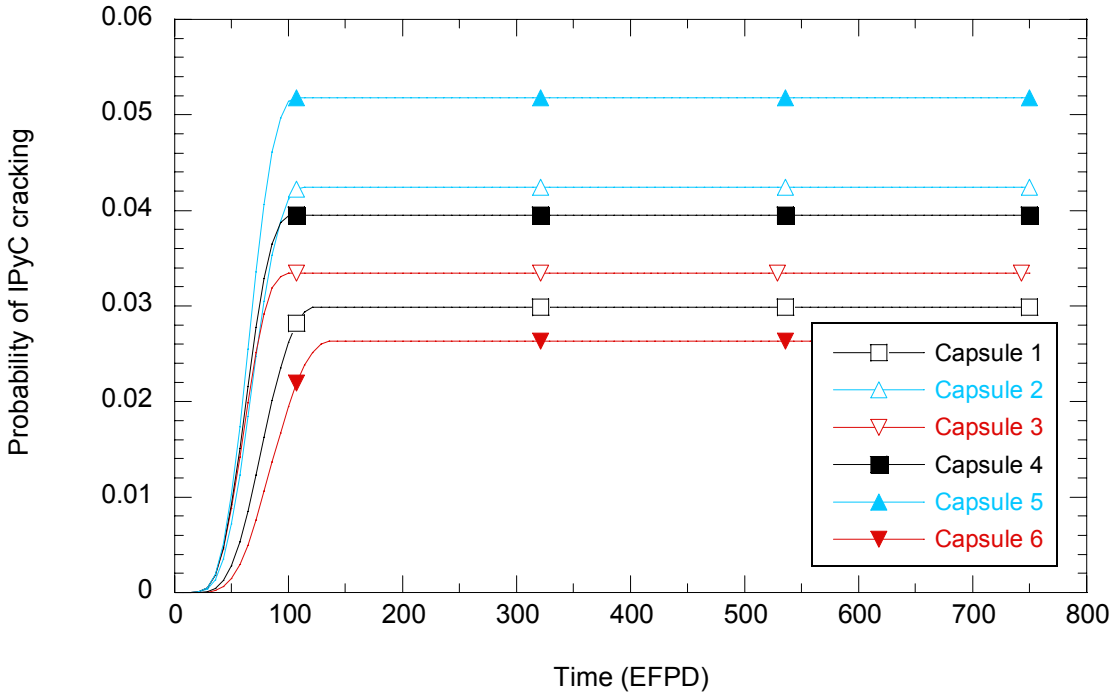

Figure 23. IPyC cracking probabilities assuming volume-averaged capsule temperatures.

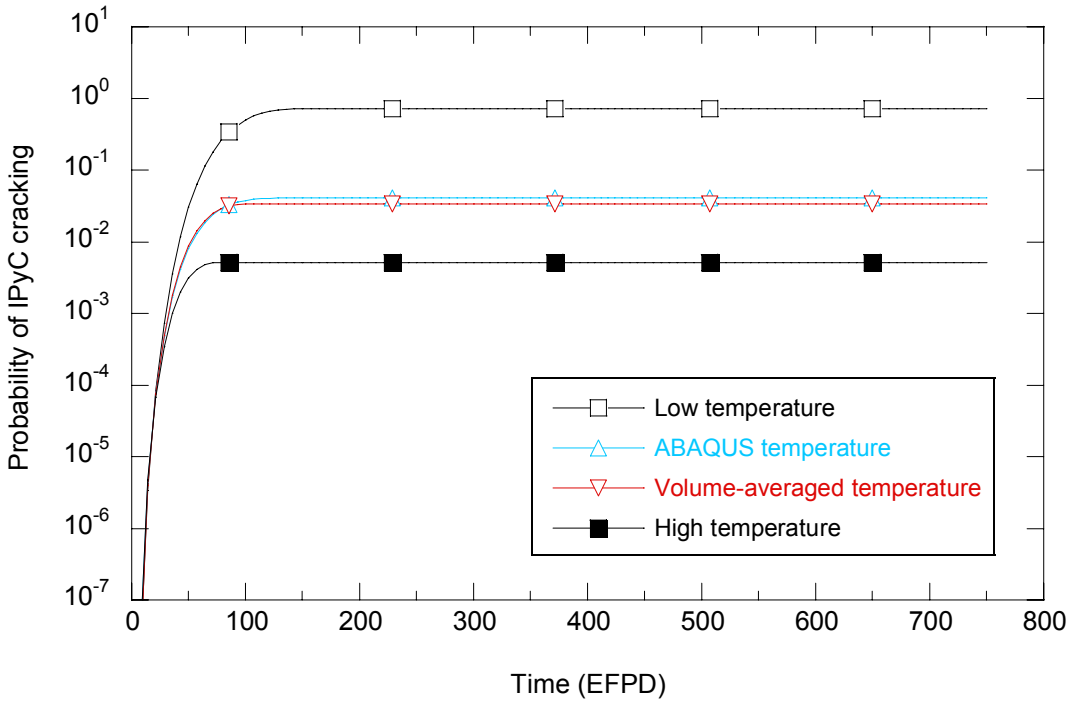

Figure 24. Capsule 3 IPyC cracking probabilities for various capsule temperatures.

consistent with those predictions. R/B results relative to capsule-to-capsule differences for Kr-85m are given in Figure 25. Capsule 3 results for fission products with relatively short (less than 1000 s) and relatively long (greater than 1000 s) half-lives are shown in Figures 26 and 27, respectively. (It should be noted that the absence of particle failures eliminated any need for solid fission product transport calculations.)

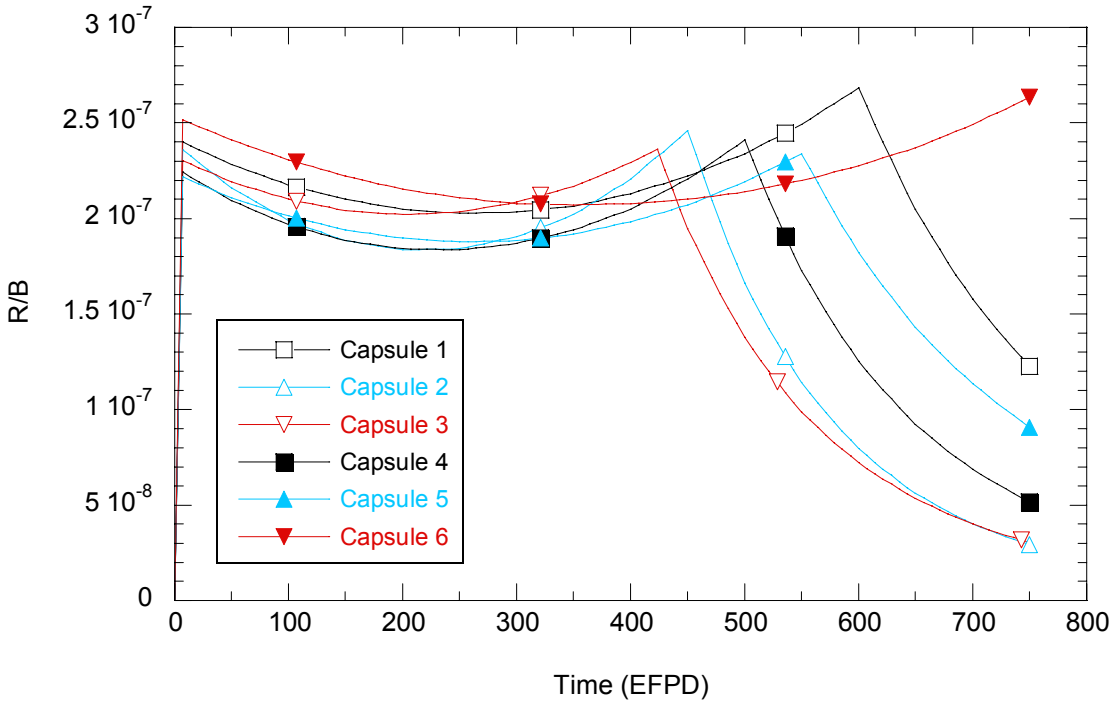

Figure 25. Kr-85m R/B results assuming volume-averaged capsule temperatures.

4. CONCLUSIONS

Fuel particle failure analyses of the AGR-1 test were completed using PARFUME. The following summarizes conclusions derived as a result of this work.

Failure probabilities are predicted to be low, resulting in a potential for failure of less than one fuel particle per capsule.

The fuel particles are exposed to relatively moderate conditions, such that none of the failure mechanisms are triggered to any meaningful degree. The predictions do show some cracking of the IPyC layer, but irradiation temperatures are at levels where these cracks do not induce significant SiC stresses.

It is worth noting that design and specification constraints were key to limiting fuel particle failures in these analyses. For example, higher anisotropy and greater asphericity would lead to higher particle failure probabilities but anisotropy and asphericity were limited by fuel specifications. Likewise, higher temperatures would lead to greater SiC layer attack by Pd but temperature was limited by the irradiation test speci-

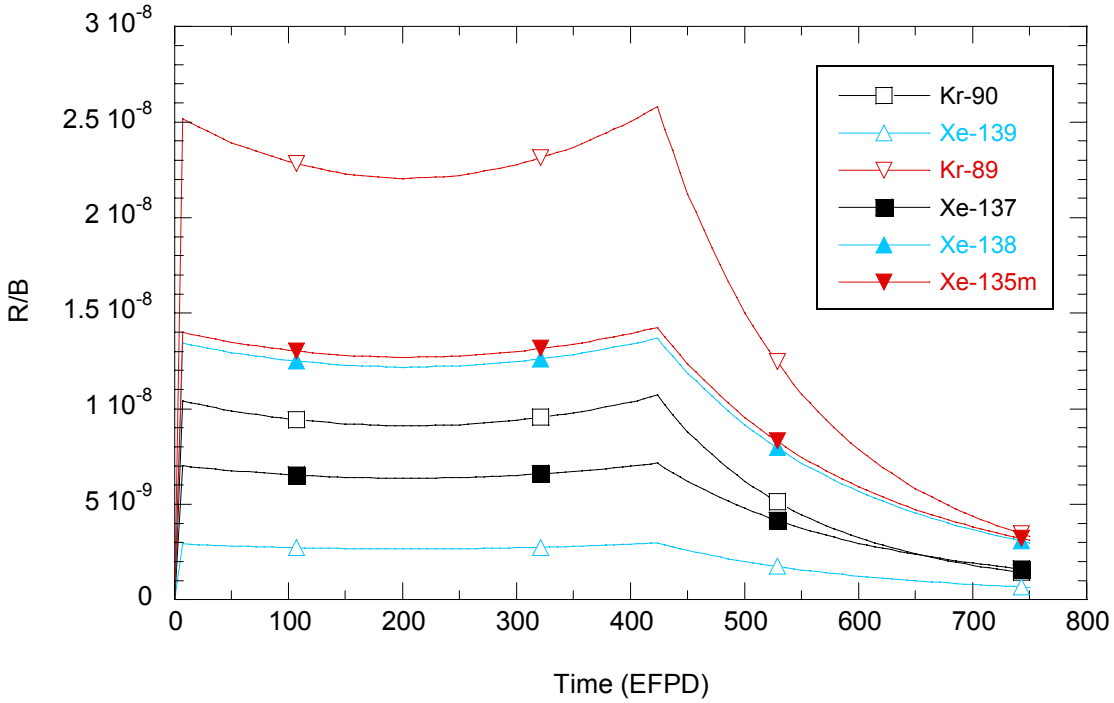

Figure 26. Capsule 3 R/B results for fission products with relatively short (less than 1000 s) half-lives assuming volume-averaged capsule temperatures.

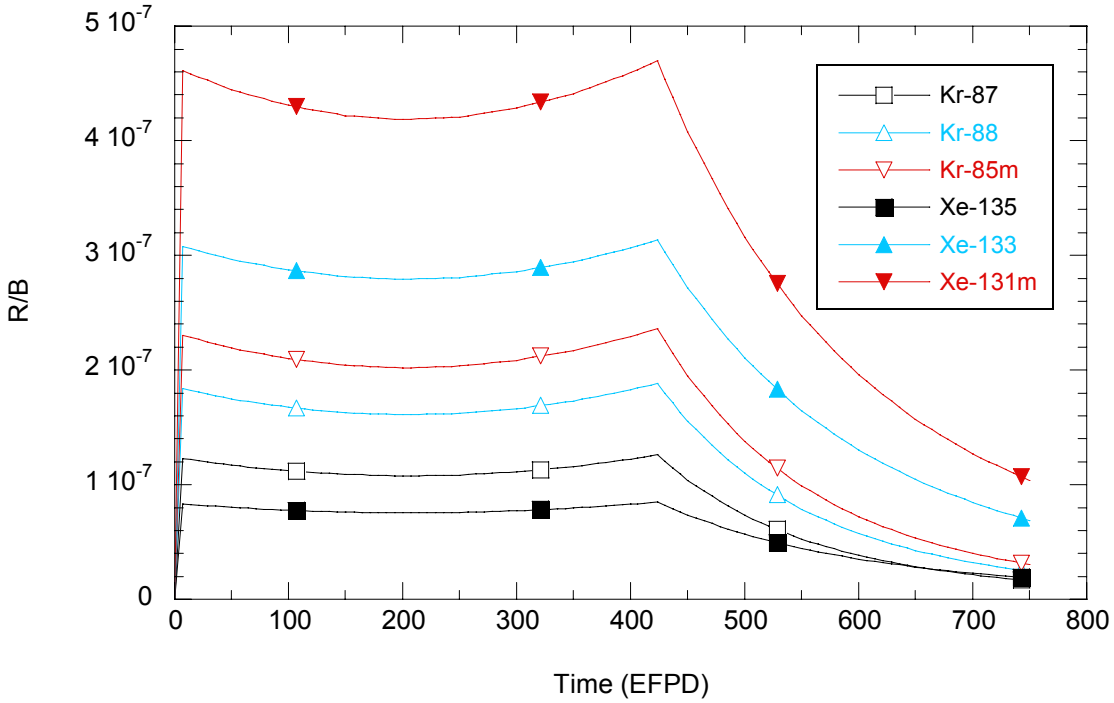

Figure 27. Capsule 3 R/B results for fission products with relatively long (greater than 1000 s) half-lives assuming volume-averaged capsule temperatures.

fication. Test train design incorporated boron carbide in the sample holders to simulate nominal conditions in a high temperature gas reactor. As a result, beginning of life power densities and thermal gradients were reduced. Therefore, constraints imposed by fuel and test specifications along with design considerations are reflected in PARFUME results such that predicted AGR-1 fuel particle failures are expected to be low.

IPyC cracking is the cause of all potential fuel particle failures.

Irradiation-induced shrinkage of the IPyC layer induces tensile stresses in the IPyC. Because of the Weibull distribution in IPyC strength, these stresses result in cracking of the IPyC for a nominal percentage of particles. For these cracked particles, the presence of the crack induces tensile stresses in the SiC layer in the region of the crack tip. With a Weibull distribution in SiC strengths, a small fraction of these cracked particles are predicted to fail.

Because a strong bond is assumed at the IPyC/SiC interface, the predictions indicate that debonding between these layers does not occur. Therefore, partial debonding of the IPyC does not contribute to the predicted failure probability. Because the internal pressures are predicted to be very small, pressure vessel failures do not contribute to the failure probability. Finally, the amoeba effect did not contribute to particle failures because UCO kernel migration coefficients are too small.

R/B ratios are very low.

R/B ratios are very low because there are no predicted particle failures contributing to fission gas release. Therefore, the only contribution to release is due to uranium contamination.

The results are not significantly affected by the statistical variations in pyrocarbon BAF, pyrocarbon densities, or particle asphericity.

Statistical variations in pyrocarbon BAF, pyrocarbon densities, and particle asphericity were reported in the AGR-1 test plan. Effects of those variations can be modeled using PARFUME. However, sensitivity calculations indicated that they have limited impact on AGR-1 fuel particle failure probabilities. Although these parameters could affect results under different irradiation conditions, they were found to be unimportant here because Weibull statistical distributions for the IPyC and SiC strength controlled the probability for IPyC cracking and the resulting failure of the SiC.

5. REFERENCES

1. Miller, G. K., and D. L. Knudson, “Advanced Gas Reactor-1 Pre-Test Prediction Analyses Using the PARFUME Code,” EDF-5741, Idaho National Laboratory, March 2005.
2. Maki, J. T., *AGR-1 Irradiation Experiment Test Plan*, INL/EXT-05-00593, Revision 2, Idaho National Laboratory, January 2007.
3. Chang, G. S., and M. A. Lillo, “Confirmatory Neutronics Analysis of the AGR-1 Experiment Irradiated in ATR B-10 Position,” EDF-7120, Revision 1, Idaho National Laboratory, February 2007.
4. Ambrosek, R. G., “Thermal Analyses for Design of AGR-1,” EDF-5138, Idaho National Laboratory, October 2005.

5. Ambrosek, R. G., data files transmitted via e-mail to D. L. Knudson and J. T. Maki, Idaho National Laboratory, January 10 and 18, 2007. (Transmitted files contained finite element calculations performed with the ABAQUS Version 6.6-1 computer program on a SUN W2100z platform.)
6. Idaho National Engineering and Environmental Laboratory, (D. A. Petti, Principal Investigator), *Development of Improved Models and Designs for Coated-Particle Gas Reactor Fuels: Final Report under International Nuclear Energy Research Initiative (INERI)*, INEEL/EXT-05-02615, December 2004.
7. Miller, G. K., J. T. Maki, D. L. Knudson, and D. A. Petti, "Current Capabilities of the Fuel Performance Modeling Code PARFUME," *2004 International Conference of High Temperature Reactor, HTR 2004*, Beijing, China, September 2004.
8. PARFUME, Version 2.12 in the Revision Control System, running on a Sun x86_64 workstation operating with SUSE LINUX, March 2007.
9. Tichy, W. F., "RCS - A System for Version Control," *Software Practice and Experience*, 15, **7**, pg. 637-654, July 1985.
10. Miller, G. K., and D. L. Knudson, "PARFUME Benchmark for Coated Particle Fuel Performance Under Normal Operation," EDF-6036, Idaho National Laboratory, June 2005.
11. Parry, J. R., "Fission Heat Rate Reduction from the Use of He-3 Coolant in the AGR-1 Experiment During a PALM Cycle," EDF-7225, Idaho National Laboratory, Draft September 2006.
12. CEGA Corporation, *NP-MHTGR Material Models of Pyrocarbon and Pyrolytic Silicon Carbide*, CEGA-002820, Revision 1, San Diego, CA, July 1993.
13. Miller, G. K., "Calculating Failure Probabilities for TRISO-Coated Fuel Particles using an Integral Formulation," EDF-7413, Idaho National Laboratory, October 2006.
14. Miller, G. K., D. A. Petti, D. J. Varacalle Jr., and J. T. Maki, "Statistical Approach and Benchmarking for Modeling of Multi-Dimensional Behavior in TRISO-Coated Fuel Particles," *J. Nuclear Materials*, **317**, p. 69-82, 2003.
15. Miller, G. K., D. A. Petti, and J. T. Maki, "Consideration of the Effects of Partial Debonding of the IPyC and Particle Asphericity on TRISO-Coated Fuel Behavior," *J. Nuclear Materials*, **334**, p. 79-89, 2004.
16. *ABAQUS User's Manual*, Version 6.4-1, Hibbitt, Karlsson, and Sorenson, Inc., 2004.
17. Hawkes, B. D., "ABAQUS Version 6.4-1 Standard and Explicit Validation and Verification," EDF-4549, February 2004.
18. Martin, D. G., "Considerations Pertaining to the Achievement of High Burnups in HTR Fuel," *Nuclear Engineering and Design*, **213**, p. 241-258, 2002.
19. Redlich, O., and J. N. S. Kwong, "On the Thermodynamics of Solutions. V. An Equation of State. Fugacities of Gaseous Solutions," *Chem. Rev.*, **44**, p. 233, 1949.
20. Reid, R. C., J. M. Prausnitz, and B. E. Poling, *The Properties of Gases and Liquids*, Fourth Edition, McGraw-Hill, Inc., 1987.
21. *HSC Chemistry User's Guide*, Version 5.0, Outokumpu Research, Oy, Finland, 2002.
22. Moore, R. L., B. G. Schnitzler, C. A. Wemple, R. S. Babcock, and D. E. Wessol, *MOCUP: MCNP-ORIGEN2 Coupled Utility Program*, INEL-95/0523, 1995.
23. Briesmeister, J. F., et al., *MCNP - A General Monte Carlo N-Particle Transport Code*, Los Alamos National Laboratory, Los Alamos, NM, 1997.

24. Croff, G., *A User's Manual for the ORIGEN2 Computer Code*, Oak Ridge National Laboratory, Oak Ridge, TN, 1980.

25. Littmark, U., and J. F. Ziegler, *Handbook of Range Distributions for Energetic Ions in All Elements*, Permagon Press, 1980.

26. Booth, A. H., *A Method of Calculating Fission Gas Release from UO2 Fuel and its Implication to the X-2-f Loop Test*, Atomic Energy of Canada Limited Report - 496, 1957.

27. Turnbull J. A., et al., "The Diffusion Coefficient of Gaseous and Volatile Species During the Irradiation of Uranium Dioxide," *J. Nuclear Materials*, **107**, p. 168, 1982.

28. Olander, D. R., *Fundamental Aspects of Nuclear Reactor Fuel Elements*, ERDA, TID-26711-P1, 1976.

29. Nabielek, H., e-mail communication discussing an unpublished document: Nabielek, H., "Partikeln und Brennelemente fur den HTR," KFA-HTA, January 1991, received November 13, 2002.

30. Rollig, K., *Release of Noble Gases and Halogens from the PBMR Core*, Westinghouse Reaktor GmbH, GBRA 052 336, 2001.

31. Miller, G. K., D. A. Petti, D. J. Varacalle Jr., and J. T. Maki, "Consideration of the Effects on Fuel Particle Behavior from Shrinkage Cracks in the Inner Pyrocarbon Layer," *J. Nuclear Materials*, **295**, p. 205-212, 2001.

32. Miller, G. K., D. A. Petti, J. T. Maki, and D. L. Knudson, "An Evaluation of the Effects of SiC Thinning on Failure of TRISO-Coated Fuel Particles," *J. Nuclear Materials*, **355**, p. 150, 2006.

33. Petti, D. A., and J. T. Maki, "Irradiation Temperature for AGR-1,", EDF-5016, Idaho National Laboratory, July 2004.